Failure of Unrestrained Lightly Reinforced Concrete Slabs Under Fire – Part II: Verification and Application

E. Omer[1], B.A. Izzuddin[2] and A.Y. Elghazouli[3]

Abstract

The simplified analytical models developed in the companion paper for the failure assessment of simply supported composite floor slabs without planar restrained are investigated further in this paper. In addition to taking account of membrane action and the material response at elevated temperature, these models allow for the bond developed between the reinforcement and the surrounding concrete. This is an essential requirement for defining a rational performance-based failure criterion for for composite floor slabs at elevated temperatures, since bond along with the characteristics of the reinforcement response govern failure by rupture of the reinforcement across full depth cracks. The kinematic assumptions inherent in the formulation of the complete and simplied variants of the models are first verified against detailed finite element analysis, and comparisons are made against a previously proposed model to identify common features and important benefits. Subsequently, the models are utilised in several examples which demonstrate their applicability, and the treatment of important factors related to boundary conditions and geometric configuration is discussed, highlighting in the process any restrictions on the application of the proposed models.

[1] Research student, Dept. Civil & Env. Eng'g, Imperial College London SW7 2AZ.
[2] Professor of Computational Structural Mechanics, Dept. Civil & Env. Eng'g, Imperial College London, SW7 2AZ, (Corresponding author, b.izzuddin@imperial.ac.uk), M.ASCE
[3] Reader in Engineering Structures, Dept. Civil & Env. Eng'g, Imperial College London SW7 2AZ, M.ASCE

1 Introduction

With advances in computational capabilities, comprehensive procedures were developed [1] to evaluate conditions which have traditionally been neglected in design such as explosion and fire. However, for design purposes, models which are simple to use are prefered. These models though, should be able to account rationally for important effects, removing any reservations related to their validity and conservativeness [2]. In this respect nonlinear finite element procedures can be employed in order to enhance our understanding of structural behaviour and validate analytical models which are aimed at representing design cases in a simple manner.

Among others issues, the fire resistance of composite floor slabs used in modern office buildings has received considerable attention over the recent years following reals events where their ability to resist the imposed load beyond expected was observed. Experimental programs have furtherly established these observations and served as benchmarks for the development of numerical and analytical procedures.

Nevertheless, current models used for the assessment of capacities of such slabs fail to address the important feature of light reinfocement and bond stresses. A concrete member is defined as lightly reinforced if the cracking capacity of the concrete is larger than the ultimate tensile capacity of the reinforcement. These issues were addessed in subsequent models [2] which were developed for the failure assessment of lightly reinforced concrete (LRC) beams under elevated temperatures. Nevertheless, due to their complexity these models are not suitable for the failure assessment of slabs by designers.

In the companion paper [3], two variants of an analytical model are presented in order to model the failure under elevated temperature of composite slabs which are supported vertically along the edges but do not exhibit any planar restraints. These two variants are developed because failure modes observed experimentally have not so far been adequetly examined in terms of the parameters governing the likelihood of occurence of one failure mode over the other. The models developed have been extended to account for the effect of elevated temperatures and simplified forms of these models have been shown to compare favourably with the more complex complete formulations.

In the present paper, assumptions made in the formulation of the aforementioned models

are furtherly examined and the applicability of current models is demonstrated.

Finally, the simplified slab models given in the companion paper , which have been shown to combine practicality and accuracy, are presented systematically in order to facilitate their application in design practice. The application of the proposed models and any restrictions are also discussed, and examples are presented demonstrating their applicability.

2 Verification of Kinematics of Unrestrained Slab Models

The kinematic assumptions adopted for the two CM and IM variant models proposed in the companion paper [3] for unrestrained floor slabs under fire are verified here using the nonlinear finite element analysis program ADAPTIC [1]. In ADAPTIC, the finite element employed for composite and reinforced concrete floor slabs [4] is formulated using the smeared crack approach, which normally represents well reinforced slabs where multiple cracks occur. However, for the case of LRC members, where only a single crack along a certain region occurs, the stresses in the reinforcement can be affected by the the mesh size and can lead to unrealistically high strain and consequently stress concentrations [6]. In addition to this, the ADAPTIC element [4] assmes full bond, thus neglecting the finite bond strength between the reinforcement and the surrounding concrete, and therefore it cannot be employed for full verification of the present simplified models. Nevertheless, ADAPTIC can be used to verify the accuracy of the kinematic expressions of the proposed model by neglecting the strain hardening of the steel reinforcement. In this way, the stress in the reinforcement across the crack does not exceed the yield strength of steel, and the response predicted by ADAPTIC becomes insensitive to the selected mesh size and can be compared against the response obtained using the proposed simplified models.

Towards this end, a $12\times6m^2$ LRC slab is analysed with ADAPTIC using the *csl4* element [4],[5], where due to symmetry only a quarter model is considered. In-plane translations along the simple edge supports are allowed, and appropriate translational/rotational restraints are applied along the lines of symmetry. A mesh of 16×8 square elements is used with a corresponding element side size of $375mm$, and the reinforcement is located at the element mid-height where restraints are applied, corresponding to the assumption that the slab is supported at the level of the reinforcement. The geometric and steel material properties of the slab, defined in

the companion paper [3], are given in Table 1.

In order to simulate with ADAPTIC the crack pattern of the failure modes postulated by the proposed models, the tensile strength and stiffness of concrete assigned for the elements at the locations coinciding with the the yield lines is set to a small value compared to that for the rest of the elements. The material properties for the ADAPTIC steel model *stl4* [5] are given in Table 2 and for the concrete model con11 [5] are provided in Table 3 and Table 4 [2],[6]. This imposes a yield line pattern which is in line with experimental results and the current analytical model formulation, thus enabling the verification of the proposed simplified models for the large displacement response under the prescribed yield pattern. Accordingly, a successful comparison would establish the accuracy of the kinematic descriptions of the proposed models and their ability to model the large displacement response for the considered deformation modes.

The deflected shapes of the slab corresponding to the crack locations assumed by the two variant models, CM and IM, are shown in Figures 1 and 2 for a central deflection of $600mm$. It is evident from these figures the cracks open at the locations intended. Moreover, it can be observed from Figure 1 that the crack along the central yield line is wider closer to the intersection of the yield line, which is in line with the kinematic assumption of the CM model.

The load-deflection responses obtained from ADAPTIC and the developed models are presented in Figure 3, where it is clear that the predictions of both variant models compare very favourably against the numerical predictions of ADAPTIC. Therefore, this verifies the accuracy of the kinematic assumptions of the two model variants, providing the necessary level of confidence for their use in the assessment of unrestrained LRC slabs including the influence of membrane action.

3 Comparison against BRE Model

The proposed slab CM model is compared here against the previously developed BRE model **Error! Reference source not found.**, which is based on the following assumptions:

- the slab is simply supported but free to move in-plane,
- cracks are developed at locations predicted by yield line theory,
- the slab parts bounded by the yield lines and the support rotate around them in a rigid

manner,

- a full depth crack is developed perpendicular to the long span dividing the slab into two equal parts,
- the reinforcement spanning across the yield lines is assumed to be at yield (Figure 4), while the reinforcement across the full depth crack is assumed to have reached the ultimate strength of the steel, with $f_{ultimate} = 1.1 f_{yield}$,
- the compressive forces in the concrete are assumed to be constant along the central yield line, and increasing along the diagonal yield line to a higher value at the slab corners,
- the compression along the full depth crack is assumed to be concentrated at the edge of the slab,
- a moment-axial force interaction law is adopted, implicitly defining the centre of bending over a section,
- the in-plane and out of plane equilibrium of the slab parts is used for the formulation of the enhanced slab capacity under larger displacements,
- the enhancement due to the membrane forces, including their effect on the moment capacity, is incorporated in addition to the yield line theory capacity of each of the triangular and trapezoidal parts of the slab,
- the contribution of the two parts of the slab are combined to give the total slab capacity using a relationship proposed by [9], which accounts for the effect of out-of-plane shear forces.

In comparing the proposed model with the BRE model, some minor modifications have been necessary for a valid comparison. In the current formulation of the CM model, it is assumed that the full-depth crack opens at the centre of the slab, and that the adjacent trapezoidal parts are in contact at the centre of the slab at the top fibre. A direct comparison between the proposed CM model and the BRE model shows discrepancies, which are attributed to the fact that the CM model is based on a single degree of freedom kinematic displacement approach, whereas the BRE model is based on an equilibrium approach employing an assumed stress state. To establish more clearly the sources of discrepancy, the proposed CM model is expressed using the equilibrium approach in which case the compressive forces in the concrete are concentrated at the three points of contact between the trapezoidal part and the adjacent parts. These

compressive forces are then distributed to correspond more closley to the BRE model, thus allowing the determination of whether the discrepancies between the proposed CM model and the BRE model are largely due to the difference between the effective and assumed internal stress distributions, respectively.

To enable a direct comparison, it is assumed with the BRE model that the stress of the reinforcement along the full depth crack is equal to the yield strength, while the influence of strain hardening is ignored with the proposed kinematic CM model. Moreover, since the CM model assumes that the slab parts are in contact at the top fibre, the centre of rotation with the BRE model is taken at the top fibre. Finally, the relationship combining the contribution of the triangular and trapezoidal parts of the BRE model is modified in order to match the equivalent equilibrium formulation to the proposed CM model.

3.1 Equilibrium formulation with concentrated compression

This formulation simply expresses the proposed kinematic CM model using an equilibrium approach, where concentrated compressive forces are considered at the three contact points. Referring to Figure 5 and considering planar rotational equilibrium of the trapezoidal part about the bottom left corner, the compression at the top fibre at the centre of the slab C_1 is given by:

$$C_1 = T_y \frac{a}{4} \tag{1}$$

Considering the out-of-plane rotational equilibrium of the tranpezoidal part about the long supported edge and the triangular part about the short supported edge, both with respect to the top fibre, the following respective equilibrium conditions are obtained:

$$T_y\left(\frac{a}{2}-\eta a\right)(U_c+U_{1'})+T_y\eta a\left(\frac{U_c}{2}+U_{1'}\right)-V\frac{b}{2}-\frac{q_c a b^2}{48}(3-4\eta)-C_1U_c=0 \tag{2}$$

$$T_y\frac{b}{2}\left(\frac{U_c}{2}+U_{2'}\right)+V\eta a-\frac{q_c\eta^2a^2b}{12}=0 \tag{3}$$

where the out-of-plane shear force V is assumed to act at the intersection of the diagonals. In the above, $U_{1'}$ and $U_{2'}$ are the vertical distances between the top fibre and the level of reinforcement at the deflected configuration for the trapezoidal and triangular part respectively and are given by:

$$U_{1'} = \sqrt{1 - \frac{4U_c^2}{b^2}}d \tag{4}$$

$$U_{2'} = \sqrt{1 - \frac{U_c^2}{\eta^2 a^2}}d \tag{5}$$

The load-deflection relationship can be obtained as the solution of the two previous equilibrium equations as:

$$q_c = \frac{6T_y}{\eta\alpha^2 b^2(3-2\eta)}\left[(2\eta\alpha^2 - 4\eta^2\alpha^2 + 1)U_c + 4\eta\alpha^2 U_{1'} + 2U_{2'}\right] \tag{6}$$

where:

$$\alpha = \frac{a}{b} \tag{7}$$

$$\eta = \frac{1}{2\alpha^2}\left(\sqrt{3\alpha^2 + 1} - 1\right) \tag{8}$$

3.2 Equilibrium formulation with distributed compression

As an enhancement of the previous assumption of concentrated compression, it is assumed here that the concrete compression is distributed along the yield lines at the top fibre (Figure 6). The compression is constant along the central yield line, and increasing along the diagonal yield line towards the slab corner. Again, the reinforcement stress is at yield along the cracks, and the vertical shear force between the triangular and trapezoidal force is assumed to be concentrated at the intersection of yield lines. The load-deflection relationship can be obtained

by solving the following simultaneous equations of equilibrium, which respectively correspond to translational equilibrium of the trapezoidal part in the longitudinal direction, translational equilibrium of the triangular part in the transverse direction, planar rotational equilibrium of the trapezoidal part, rotational equilibrium of the trapezoidal part about the longitudinal axis and rotational equilibrium of the triangular part about the transverse axis:

$$(T_y - \sigma_1)\frac{a}{2} + \frac{(\sigma_1 - \sigma_2)\eta a}{2} - S\cos\theta = 0 \tag{9}$$

$$T_y \frac{b}{2} - \frac{(\sigma_1 + \sigma_2)b}{4} + S\sin\theta = 0 \tag{10}$$

$$T_y \frac{a^2}{8} - \frac{\sigma_1}{2}\left(\frac{a^2}{4} - \eta^2 a^2\right) - \frac{2\sigma_1 + \sigma_2}{6}\left(\eta^2 a^2 + \frac{b^2}{4}\right) = 0 \tag{11}$$

$$(T_y(U_c + U_{1'}) - b_1 U_c)\left(\frac{a}{2} - \eta a\right) + T_y \eta a\left(\frac{U_c}{2} + U_{1'}\right) - V\frac{b}{2} - \sqrt{\eta^2 a^2 + \frac{b^2}{4}}\,\frac{2\sigma_1 + \sigma_2}{6}\sin\theta U_c - q_d\left(\frac{a}{2} - \eta a\right)\frac{b^2}{8} - \frac{q_d \eta a b^2}{24} = 0 \tag{12}$$

$$T_y \frac{b}{2}\left(\frac{U_c}{2} + U_{2'}\right) + V\eta a - \sqrt{\eta^2 a^2 + \frac{b^2}{4}}\cos\theta U_c\,\frac{2\sigma_1 + \sigma_2}{6} - \frac{q_d \eta^2 a^2 b}{12} = 0 \tag{13}$$

where $U_{1'}$ and $U_{2'}$ are given in Equations (4)-(5).

Solving the above equations, the load-deflection relationship is obtained as:

$$q_d = \frac{6T_y}{b^2}\frac{(4\eta\alpha^2 - 3\alpha^2 - 1)(4\eta\alpha^2 U_{1'} + 2U_{2'}) + (12\eta^2\alpha^2 - 8\eta\alpha^2 - 1)U_c}{\left(18\eta\alpha^2 + 2\eta - 8\eta^2\alpha^2 - 9\alpha^2 - 3\right)\eta\alpha^2} \tag{14}$$

in which α and η are given by Equations (7) and (8).

3.3 Modified BRE model formulation

Considering the discussion in Sections 3.1 and 3.2, the enhanced load capacity q of an unrestrained slab according to the BRE model [7], [8] is given by:

$$q = eq_y \tag{15}$$

where e is a non-dimensionless enhancement factor with respect to the yield line capacity q_y given by:

$$e = e_1 - \frac{e_1 - e_2}{1 + 2\alpha^2} \tag{16}$$

In the above equation, e_1 and e_2 represent the enhancement in the load capacity for the trapezoidal (denoted by subscript 1) and the triangular (denoted by subscript 2) parts, respectively (Figure 4), and these are obtained by considering independently the out-of-plane moment equilibrium of each part. The enhancement factors for each slab portion include the contribution of both membrane and bending effects and are given by [8]:

$$e_1 = e_{1m} + e_{1b} \tag{17}$$

$$e_2 = e_{2m} + e_{2b} \tag{18}$$

where,

$$e_{1m} = \frac{4b_c U_c}{d(3 + g_o)} \left[1 - 2\eta + \frac{\eta(2 + 3k - k^3)}{3(1 + k)^2} \right] \tag{19}$$

$$e_{1b} = 2\eta \left[1 + \frac{\alpha_i b_c}{2}(k - 1) - \frac{\beta_i b_c^2}{3}(k^2 - k + 1) + (1 - 2\eta)(1 - \alpha_i b_c - \beta_i b_c^2) \right] \tag{20}$$

$$e_{2m} = \frac{4b_c U_c}{d(3 + g_o)} \left[\frac{\eta(2 + 3k - k^3)}{6(1 + k)^2} \right] \tag{21}$$

$$e_{2b} = 1 + \frac{\alpha_i b_c}{2}(k - 1) - \frac{\beta_i b_c^2}{3}(k^2 - k + 1) \tag{22}$$

In Equations (19)-(22) subscript m refers to membrane effects while subscript b refers to

bending effects. Moreover, the parameters k and b_c are obtained by considering the in-plane equilibrium of the slab parts, where α_i and β_i describe the moment-axial force interaction curve of the cross-section, and these parameters are given by:

$$k = \frac{4\eta\alpha^2(1-2\eta)}{4\eta^2\alpha^2+1}+1 \tag{23}$$

$$b_c = \frac{1.0}{8(A+B+C+D)} \tag{24}$$

$$\alpha_i = \frac{2g_0}{3+g_0} \tag{25}$$

$$\beta_i = \frac{1-g_0}{3+g_0} \tag{26}$$

in which g_0 reflects the location of the centre of rotation of the cross section taken as 1 for the top fibre and 0 for the centre of the cross section. Moreover [9]:

$$A = \frac{1}{8(1+k)}\left\{\frac{1}{2\eta}-\left(4\eta^2\alpha^2+1\right)\left[\frac{1-2\eta}{2\eta}+\frac{1}{3(1+k)}\right]\right\} \tag{27}$$

$$B = \frac{k^2}{8(1+k)}\left[2\eta^2\alpha^2-\frac{k}{3(1+k)}\left(4\eta^2\alpha^2+1\right)\right] \tag{28}$$

$$C = \frac{1}{16\eta}\left(k-1\right) \tag{29}$$

$$D = \frac{\alpha^2}{4}\left(1-2\eta\right)^2 \tag{30}$$

Equation (16) was originally proposed by Hayes [9], suggesting that it accounts for the shear force interaction between the slab portions, though the derivation of the equation was not presented. Therefore, a new approach is presented here taking into account the vertical shear force between the two slab portions similar to the approach adopted in Sections 3.1 and 3.2. The

enhancement factors for the slab parts are then combined using the equation suggested hereafter, which enables a direct comparison between the models.

The load capacities q_1 and q_2 for the individual slab parts ignoring the vertical shear interaction between them are obtained from:

$$A_1 = B_1 q_1 \tag{31}$$

$$A_2 = B_2 q_2 \tag{32}$$

where A_1 and A_2 are the moments created by the internal stress distribution, while B_1 and B_2 are the first moments of area, corresponding to the trapezoidal and triangular part, respectively, with respect to the relevant supports, as given by:

$$B_1 = \frac{ab^2}{16} - \frac{\eta ab^2}{12} \tag{33}$$

$$B_2 = \frac{\eta^2 a^2 b}{12} \tag{34}$$

By taking into account the vertical shear V the load capacity q is obtained from the following:

$$A_1 - V\frac{b}{2} = B_1 q \tag{35}$$

$$A_2 + V\eta a = B_2 q \tag{36}$$

It should be noted that the vertical shear V is assumed to be acting at the intersection of the yield lines as a concentrated force. The shear can also be assumed to be uniformly distributed along the diagonal yield line, in which case the moment generated with respect to each support would still be the same. Solving simultaneously Equations (31)-(36) the load capacity is obtained as:

$$q = \frac{(3-4\eta)q_1 + 2\eta q_2}{3-2\eta} \tag{37}$$

For comparison purposes, a modified version of the BRE model is considered which is based on the above proposed equation, leading to the following enhancement factor:

$$e = \frac{(3-4\eta)e_1 + 2\eta e_2}{3-2\eta} \tag{38}$$

instead of the original expression [9] given by Equation (16).

3.4 Comparisons

The load-deflection response of a slab is obtained here using the proposed kinematic CM model [3], the two variations based on this model considering the equilibrium approach, and the BRE equilibrium model [8] with the modified load shared between the triangular and trapezoidal parts. For the CM model, the force in the reinforcement is assumed constant at T_y throughout the loading, so as to facilitate comparison with the other models, leading to:

$$q = \frac{24T_y}{ab(3-2\eta)}\left(\int_{\eta a}^{a/2} \frac{\mathrm{d}\Delta_{sce}^c}{\mathrm{d}U_c}\mathrm{d}x + \int_0^{\eta a} \frac{\mathrm{d}\Delta_{sdy}^c}{\mathrm{d}U_c}\mathrm{d}x + \int_0^{b/2} \frac{\mathrm{d}(\Delta_{sdx}^c + \Delta_{scr}^c)}{\mathrm{d}U_c}\mathrm{d}y \right) \tag{39}$$

For the other three models, the load-deflection response is obtained in accordance with Sections 3.1, 3.2 and 3.3. For the parameters given in Table 5, the obtained results are plotted in Figure 7. Since the equilibrium variations of the CM model assume that the concrete remains completely rigid, which forces the centre of rotation of the cross section to be at the top fibre, g_0 is set to 1 in order to facilitate direct comparison with the BRE model. This results in a yield line capacity of $10.2 kN/m^2$.

It can be observed that for all depicted models the initial load resistance corresponds to a value very close to the yield line capacity. Moreover, the predictions of the kinematic CM model

and its equilibrium variant assuming concentrated compression forces are very similar, especially at lower displacements, thus verifying that the kinematic and equilibrium models are equivalent.

Furthermore, the modified BRE model compares favourably with the equilibrium variant of the CM model assuming distributed compression forces, both predicting a less stiff response in comparison with the concentrated compression kinematic equilibrium model.

The above comparisons demonstrate that the discrepancies observed between the proposed CM kinematic model and the BRE equilibrium model are mainly due to the assumption of rigid compressive concrete in the CM model, leading to discrete points of contact. These discrepancies may however be reduced for the CM model by moving the points of contact inwards along the yield lines and along the through depth crack as well as down from the top extreme fibre, though this is not attempted in the present work. This is because there is no guarantee that the equilibrium model, which is based on an assumed stress state, is more accurate in the general case when the stresses in the steel reinforcement vary due to strain hardening combined with bond effects.

4 Validation against BRE Experiment

In this section, the proposed models are compared against a test that was performed at BRE [10] on a simply supported composite slab without planar restraint, for which the effect of elevated temperature was simulated by removing the steel deck. The slab was uniformly loaded, and the test was terminated when a central full depth crack was developed in the short span direction, and the reinforcement across this crack ruptured. The properties of the slab as measured are given in Table 6, while the bond strength is taken as $\sigma_b = 0.156 N/mm^2$ (bond strength per unit width per unit length), which for the reinforcement used corresponds to approximately $1.67 N/mm^2$ (bond strength per unit reinforcement surface area). It should be noted that the bond strength values used here is obtained from BS8110 [13] for plain reinforcement bars since there are no bond strength values reported.

The load-deflection response is plotted in Figure 8, where it can be observed that the two proposed models [3] predict a stiffer response compared to the BRE model. It is also evident that the CM model compares particularly well with the test results which conforms to the

experimental observation of a central through-depth crack. Moreover, Table 7 demonstrates that the failure prediction of the current CM formulation is conservative compared to the experimentally observed failure point. From the same table it is also evident that the BRE model gives almost identical failure deflection prediction as the test result which is due to the fact that the BRE model has been specifically calibrated against this test. Therefore, it can be concluded that the proposed models can realistically capture the failure of LRC slabs, predicting the failure load and displacement at reinforcement rupture using sound engineering principles.

5 Application of Proposed Models for Fire Conditions

Here, the simplified elevated temperature models for unrestrained slabs proposed in the companion paper [3] along with the model for restrained slabs developed previously [11] are considered, and their applicability is demonstrated with two examples. In each case, the deflection-temperature response for a constant load and the failure load-temperature curve are obtained for the restrained slab model and the two variants of the unrestrained slab model. The only parameter changing between the two examples is the length of the short span. The composite slabs are of a corrugated shape typically adopted in modern office buildings (Figure 9); however, the contribution of the steel decking and any secondary steel beams is neglected, since in the event of a fire such contributions become small especially at failure when the temperatures are high. The reinforcement chosen consists of the A142 mesh corresponding to bar of $6mm$ diameter placed at $200mm$ centres placed at a depth of $d = 45mm$ from the top of the slab. It is assumed that lightweight concrete with a compressive strength of $30N/mm^2$ is used resulting in a slab self weight of $2.3kN/m^2$. It is also assumed that the reinforcement is hot rolled with a characteristic yield strength of $500N/mm^2$.

For the steel model, the stress-strain response proposed by Eurocode 4 Part1-2 [12] is adopted. The ultimate strength of the steel at ambient temperatures is specified as 25% higher than the yield strength. Moreover, it is specified that after a strain of 15%, steel exhibits strain softening. Using this information, and assuming that the stress-strain response can be approximated as bi-linear, the hardeding modulus can be obtained. Moreover, for elevated temperatures the reduction factors suggested in Eurocode 4 [12] are adopted, where the yield

strength at elevated temperture is taken as the strength corresponding to the proportionality limit of the steel. The bond strength at ambient temperatures is taken as $0.156 N/mm^2$ corresponding to $1.67 N/mm^2$ of reinforcement perimetric bond strength as specified by BS8110 [13]. Due to the lack of information the variation of bond strength with temperature, its variation is assumed to be similar to that of the compressive strength of light weight concrete as given by Eurocode 4 [12]. The variation of the material properties with temperature for the considered examples is depicted in Figure 10 and 11.

The long span of the two considered slabs is taken as $7.5m$ whereas for the first example the short span is taken as $4.5m$ and for the second as $5.5m$. The yield line capacity at ambient temperature is $2.39 kN/m^2$ and $1.85 kN/m^2$ for the two slabs respectively. It should be noted that these capacities ignore the contribution of the supporting secondary beams and the steel deck, in line with the assumption of negligible contribution at elevated temperature. The material and geometrical properties of the slabs are summarized in Table 8. Finally, an imposed load of $3.0 kN/m^2$, as given by Eurocode 1 [14],[15] for a typical office building, is considered, leading to a total load of $5.3 kN/m^2$.

The failure load-temperature responses for the two slabs are depicted in Figures 12 and 13, as obtained obtained from a family of load-deflection responses for different temperatures. The predictions of the restrained slab model [11] are denoted as RM, of the unrestrained slab central crack model as CM, and of the unrestrained slab intersection crack model as IM. Moreover, for simplicity it is assumed that the thermal curvature varies linearly from 0 to $\kappa = 4 \cdot \alpha_c$ at a temperature of $1000^0 C$ which translates to a temperature gradient of $400^0 C$ over a depth of $100mm$.

It can be observed for both slabs in Figures 12 and 13 that the capacity of a fully restrained slab is greater than the capacity of an unrestrained slab. Moreover, it is noted that the capacities of the slabs increase, especially for the restrained slab, for the lower range of temperatures up to $300^0 C$. This is attributed to the fact that the ultimate strength of steel decreases according to Eurocode 4 [12] after $300^0 C$, whereas up to that temperature the differential expansion between the reinforcement and the concrete relieves the stress in the steel for both the restrained and unrestrained slabs, while thermal expansion increases deflection and membrane action for the restrained slab.

Figures 14 and 15 depict the deflection-temperature response of the slabs under a constant uniformly distributed load of $5.5kN/m^2$, which corresponds to the total load as discussed above. Similar to the previous case, these responses are also obtained from a family of load-deflection responses for different temperatures. It is noted that for both slab spans, the restrained slab exhibits less deflections for a given temperature than the unrestrained slab. Although this might not reflect the expected result at lower temperatures, where the deflections of a restrained slab could be more due to the restraint, it depicts correctly the behaviour in the latter stages of the response where the deflection of an unrestrained slab would be more than the restrained one. Since this model does not attempt to represent the load-deflection response at the initial stages of fire loading but to capture the specific instant of failure, which clearly occurs at larger temperatures, this initial potential inaccuracy is deemed insignificant. Moreover, it is noted that increasing the short span of the slab results in a decrease in the failure temperature, which is more evident for an unrestrained slab. Finally, it is observed that the failure temperature is considerably lower for unrestrained slabs, highlighting the reserved capacity a slab acquires in the presence of planar edge restraints.

6 Model Characteristics and Restrictions

In this section, the main characteristics of the developed models [3] are discussed, and any restrictions relating to the various assumptions made in the model formulation are highlighted.

6.1 Boundary Conditions

In all the proposed models, it is assumed that there is only one layer of reinforcement, and that the slab is supported at the level of the reinforcement and is free to rotate at the supports. Furthermore, it is assumed that the reinforcement is anchored at the supports, where two variant models [3] are developed for a slab that is unrestrained against planar movement at the support, with the case of a slab subject to planar restraint considered in previous work by the authors [11].

For slabs that are adjacent to large openings or are located at the perimeter of a building, it is expected that the unrestrained slab model would provide an adequate representation of the

behaviour. On the other hand, for slabs located in the interior of a building, the restrained slab model is more appropriate, provided the stiffness and strength of the edge restraints is sufficient to prevent planar movement. Moreover, even for slabs located at the perimeter of the building, the yield line pattern adopted for the unrestrained models would have to be modified if the internal edges of the slab are sufficiently strong to prevent rotation along those edges. In any case, the unrestrained slab models proposed in this work along with the restrained slab model proposed in [11] constitute the two limiting cases of simply supported slab behaviour. In reality, none of the slabs would be completely restrained or unrestrained against planar movement, though the restrained and unrestrained slab models would define the range of expected capacity, with the actual capacity being closer to one or other of the models, depending on the actual boundary conditions.

The models also assume a single layer of reinforcement. In reality, there could be an extra layer of reinforcement over the supports providing resistance against cracking or hogging moments for the interior slabs. For an interior slab subject to large deflections, cracks also form at the supports, and the slab rotates there about the bottom fibre. Thus, additional energy is dissipated mainly at a possible top reinforcement layer, enabling the slab to sustain a higher load, and hence the proposed models would offer a conservative lower bound assessment for such cases. In any case, the modelling of a top reinforcement layer at the supports, whilst not included in the proposed models, could be incorporated by considering the additional energy dissipated in such reinforcement.

6.2 Material properties

The present models aim at providing a basis for the evaluation of the capacity of slabs under elevated temperature. Material properties which are not widely considered in conventional structural design codes, such as the bond strength between steel and concrete, the ultimate strength of the steel, and the steel hardening modulus, are needed.

Although the steel exhibits a plateau just after yielding a bilinear approximation of the steel response (Figure 16) can be made for direct use in the proposed models. The variation of the material parameters (σ_b, E_2) with temperature can also be deducted from design codes such as Eurocode 4 [12].

In addition, the present models require the bond strength, which affects the load-deflection response but more significantly the failure displacement of the slab. Generally, design codes provide values related to bond strength, but there is very little information on the bond strength at elevated temperatures. Therefore, in absence of data on bond, reduction could be related to concrete strength. This highlights the need for more experimental research to establish bond-slip characteristics at elevated temperature and its influence on the failure of floor slabs.

6.3 Applicability of proposed models

The models developed in this work are aimed at providing a tool for the assessment of LRC slabs under elevated temperature. It is assumed that the slab carries the imposed load by means of tensile membrane action combined with bending action, and failure is expected to occur in this range by rupture of the reinforcement along full depth cracks. The compressive membrane contribution of the concrete is ignored in the response, and thus the model is expected to predict lower capacity at smaller deflections, where considerable compressive arching action can occurs, particularly for slabs with planar restraint [11]. Therefore, the models are applicable provided that failure occurs following compressive arching action and within the tensile membrane action stage. Nevertheless, in the context of LRC slabs where the depth to length ratio is relatively small, it is expected that rupture of the reinforcement would not occur until well into the tensile membrane range and at relatively large deflections, as demonstrated in previous examples.

It is also assumed that the slab is lightly reinforced, and no more cracks are formed in the vicinity of an already open crack. This would be the case if the reinforcement ratio is relatively low, defined in terms of the cracking capacity of the concrete section being greater than the ultimate capacity governed by reinforcement strength. Thus, following the opening of a crack, the reinforcement would continue to carry load up to the rupture point, and the tensile stresses in the vicinity of the crack would remain below the tensile strength of concrete. Therefore, there is stress/strain concentration in the reinforcement at the crack location due to the bond stresses developed between the reinforcement and the concrete, which govern the reinforcement stress at the crack tip. This is also a valid assumption for composite slabs where typically only the minimum reinforcement ratio specified by the design codes is used, especially under elevated

temperature when the contribution of the steel deck may be ignored. Finally, the assumption of a single crack constitutes a conservative assumption, since if further cracks were to develop the strain is distributed over several adjacent cracks resulting in a delay in the rupture of reinforcement. In this case, it is likely that other failure criteria, such as compressive crushing of concrete, may govern the capacity of the floor slab.

The advantage of the proposed models lies in the fact that the deflection corresponding to reinforcement rupture can be assessed using simplified formulations which capture important parameters based on well-established engineering principles. This results in an important advancement compared to previously proposed semi-empirical methods which neglect stress concentrations [8]. Following the establishment of the failure deflection, the load corresponding to that deflection can be obtained using relatively simple expressions, and comparisons can be made against the design load of the slab to check whether the slab can sustain the specified load at a given temperature. Nevertheless, the designer has to establish whether the slab is closer to a fully restrained or to an unrestrained slab, so as to apply the relevant equations. Moreover, for the case of the unrestrained slab, since it is not clear whether the slab will fail by developing a central crack or two cracks at the intersection of the yield lines, a safe approximation would be to obtain the failure corresponding to both CM and IM variant models, and then compare the design load against the lower capacity.

7 Conslusions

A model is proposed in the companion paper for the failure assessment of simply supported lightly reinforced concrete slabs that are unrestrained against planar movement. Two variants of the model are developed adopting different failure modes, since available experimental work appears to indicate the possibility of both failure modes, and the parameters governing their formation have not yet been established. Thus, in addition to cracks at the yield line locations, the existence in the short span direction of a full depth crack at the centre of the slab or alternatively two full depth cracks at the intersection of the yield lines is formulated as two model variants. It is assumed that the slab fails by rupture of the reinforcement along these cracks. The current work does not attempt to reveal the parameters affecting the location of the full depth crack, but rather the resulting slab response following the opening of the full depth crack at either location is sought. This location affects both the load-deflection response of the

slab and the displacement corresponding to failure.

In this paper, the kinematic assumptions of the two variant CM and IM models are verified against ADAPTIC, and the differences and similarities between these models and the existing BRE model are discussed. The proposed models compare favourably with ADAPTIC and experimental results, in the latter case also providing favourable predictions of failure load and displacement.

The proposed models offer considerable advantages related to the failure assessment of composite floor slabs under fire, since it can predict the concentration of strain at crack location using fundamental engineering principles, which is especially important in the context of lightly reinforced concrete members. Previous slab models do not deal with this issue adequately, and the failure is based on semi-empirical average strain considerations thus providing results that are independent of the bond and the reinforcement response. It is demonstrated that the bond strength can affect the load-deflection response to a certain degree and the failure deflection to a far more significant extent. This is due to the fact that higher bond stresses result in higher strain concentrations at crack locations thus accelerating the failure of the slab. However, currently there are no codified values for the bond strength between the reinforcement and concrete at elevated temperatures, and the full potential of these models can only be exploited once relevant experimental studies on the bond strength have been undertaken.

In applying the proposed models, the issue of strength and stiffness of the slab surroundings should be investigated. In this respect, the conditions under which a slab can be considered restrained or unrestrained need to be identified. Furthermore, for slabs located in the interior of a building the energy dissipated at cracks developed at the perimeter of the slab may need to be included in the evaluation of the load-deflection response, though the proposed models for simply supported slabs offer a lower bound in such cases. For simply supported slabs without planar restraint, it is suggested that both the CM and IM variant models are used, and the one predicting the lowest failure load is adopted as representing the critical failure mode.

It is believed that following further research, especially related to the bond-slip characteristics under elevated temperatures, the developed models will provide the necessary tools for the adoption of performance-based failure criteria in the fire design of composite steel concrete floor slabs, and will replace the current prescriptive approaches which neglect important parameters influencing slab failure under fire conditions. Towards this end, experimental studies

are currently underway at Imperial College which aim to address this shortfall and provide the necessary data for the application of the proposed models in performance-based design of composite floor slabs under fire.

Acknowledgement

The authors would like to acknowledge the support of Dr David Moore and the funding provided by the Building Research Establishment, Watford UK, for this research.

Tables

Table 1 Geometric properties for the verification of the unrestrained slab models

h (slab height)	150mm	*a*	12000mm	A_s	$0.45\text{mm}^2/\text{mm}$
d (reinforcement depth)	120mm	*b*	6000mm	σ_b	$0.05N/mm^2$

Table 2 Material properties for *stl4*

Elastic modulus	Yield strength	Strain-hardening modulus
210 GPa	400 MPa	0.00001 × 210 GPa

Table 3 Material properties for *con11* [4],[5]

Poisson's ratio	0.2
Compressive strength	40 MPa
Shear retention factor	0.5
Shear softening parameter	0.0
Initial compressive nonlinearity parameter	0.4
Residual postrcrushing strength parameter	0.2
Compressive interaction parameter	0.6
Shear interaction parameter	0.4

Table 4 Material properties for *con11* [4],[5] affecting the opening of a crack

		CM	IM
Cracks	Elastic modulus	100 GPa	50 GPa
	Tensile strength	0.1 MPa	0.2MPa
	Tensile softening modulus	300 MPa	300MPa
No cracks	Elastic modulus	300 GPa	50 GPa
	Tensile strength	5.0 MPa	2.0MPa
	Tensile softening modulus	3000 MPa	1000MPa

Table 5 Slab properties used for comparisons with the BRE model

a	b	d	T_y
9000 mm	6000 mm	120 mm	180 N/mm
η	g_0	yield line capacity	
0.3964	1	10.2 kN/m^2	

Table 6 Geometric and material properties for the tested slab

a	$9.50m$	A_s	$0.142mm^2/mm$	T_y	$82.3N/mm$
b	$6.46m$	E_2	$500MPa$	T_u	$91.3N/mm$
d	$72mm$	σ_b	$0.156N/mm^2$	f_c	$52N/mm^2$

Table 7 Failure displacement and loads of test slab

	CM(approach 1)	CM(approach 2)	IM	BRE	Test
$U_{fc}(mm)$	186	186	175	216	223
$q_f(kN/m^2)$	4.34	4.34	3.73	3.89	4.75

Table 8 Slab properties representing realistic office buildings floor slab

a (m)	b (m)	d (mm)	$A_s(mm)$	$E_2(N/mm^2)$
7.5	4.5, 5.5	45	0.142	833
$T_y(N/mm)$	$T_u(N/mm)$	$\alpha_s(^0C^{-1})$	$\alpha_c(^0C^{-1})$	$\sigma_b(N/mm^2)$
71.0	88.8	$14\cdot10^{-6}$	$8\cdot10^{-6}$	0.156

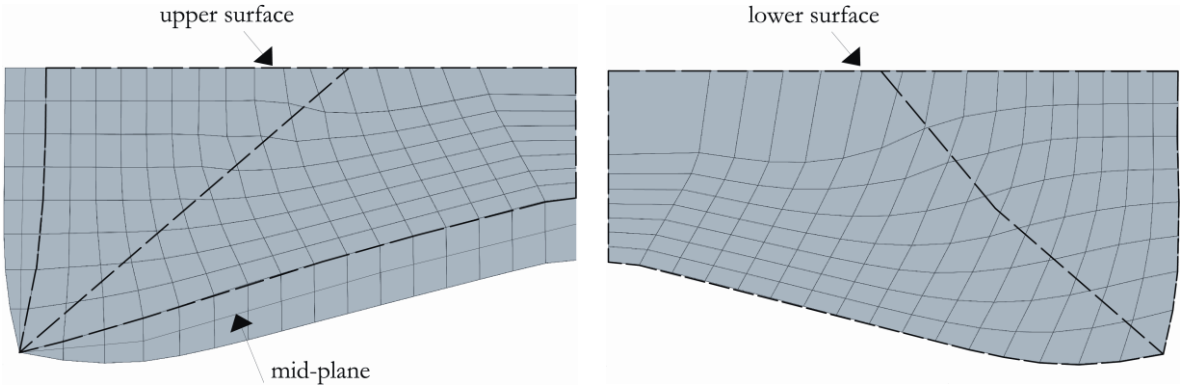

(a) top view (b) bottom view

Figure 1: Deflected shape of unrestrained slab using ADAPTIC: displacement scale=20 (CM)

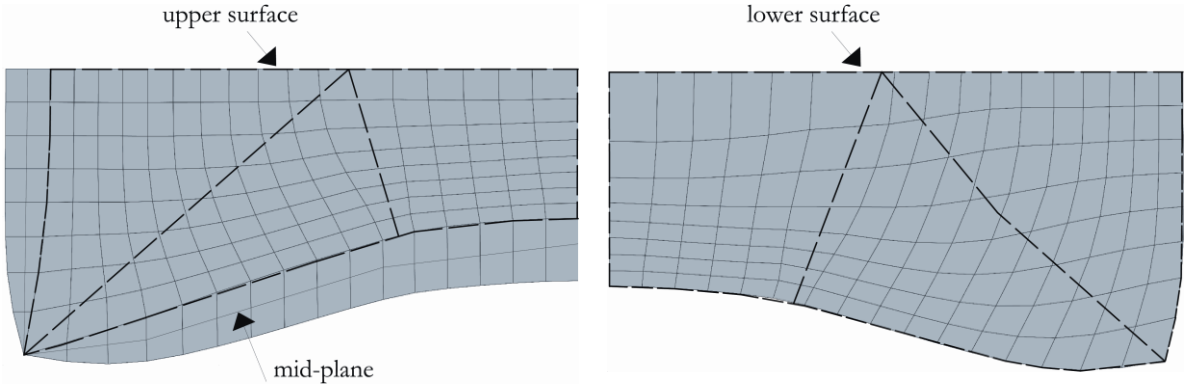

(a) top view (b) bottom view

Figure 2: Deflected shape of unrestrained slab using ADAPTIC: displacement scale=20 (IM)

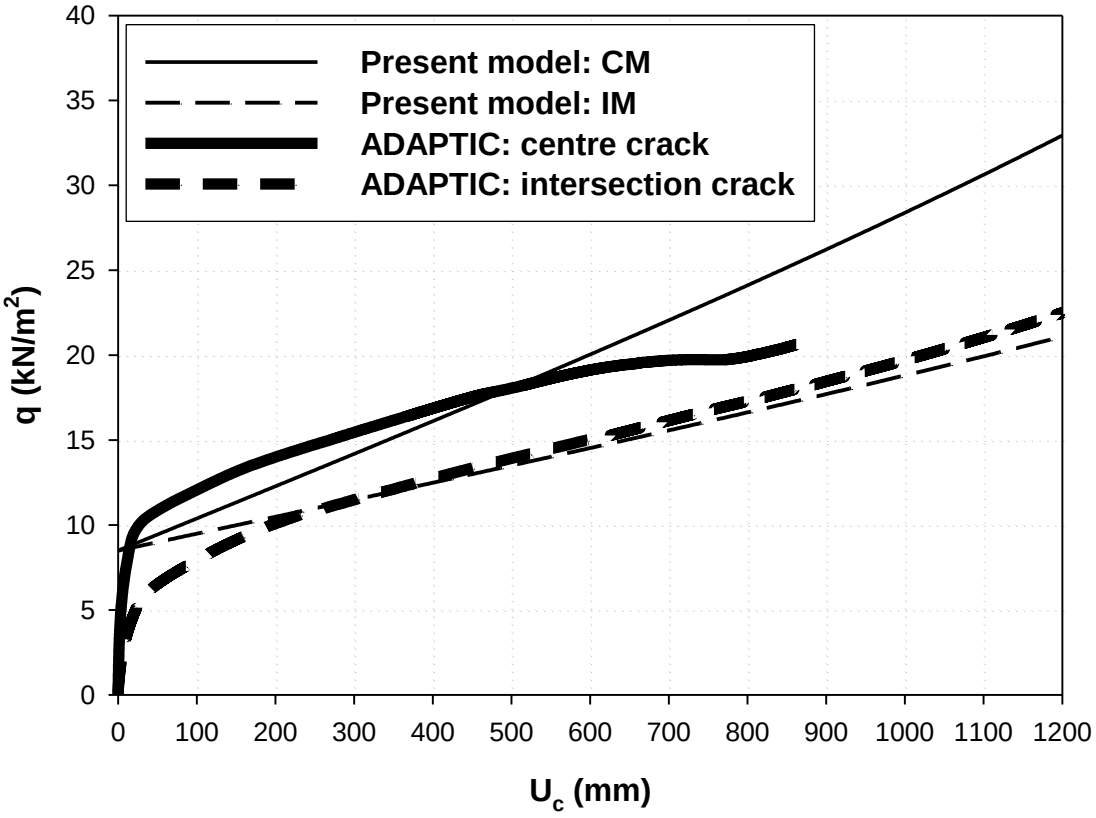

Figure 3: Load-deflection response of slab according to kinematics of CM and IM models

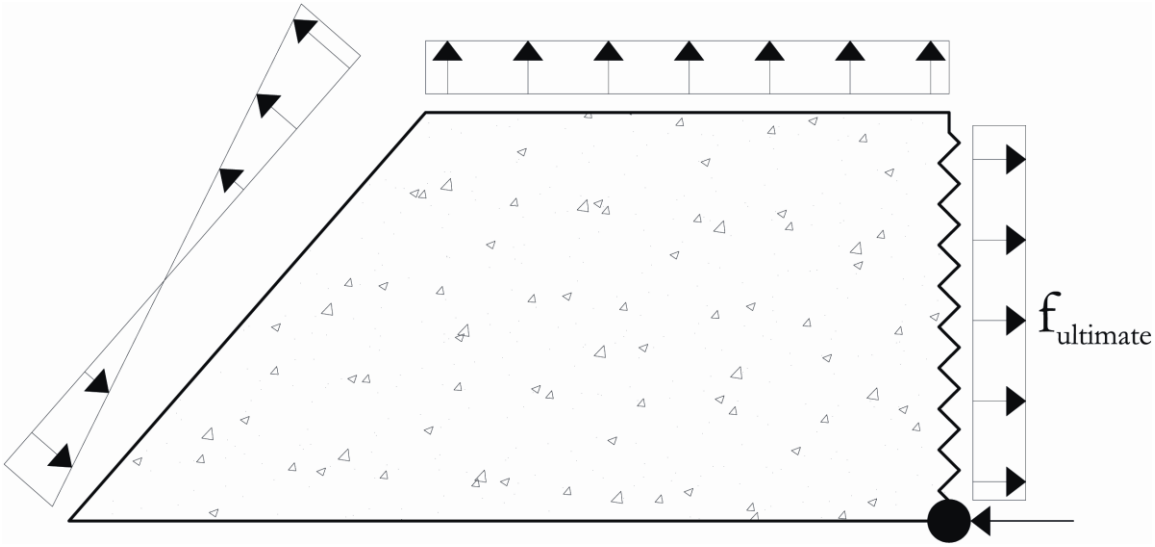

Figure 4: Resultant stress distribution assumed in the BRE model for the trapezoidal part of a quarter slab

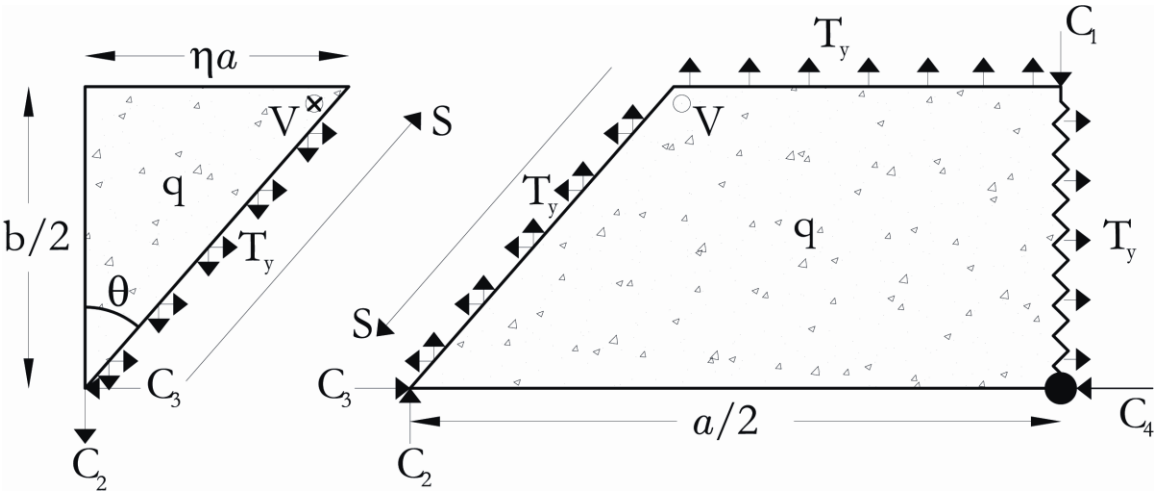

Figure 5: Stress distribution over a quarter slab for concentrated concrete compression

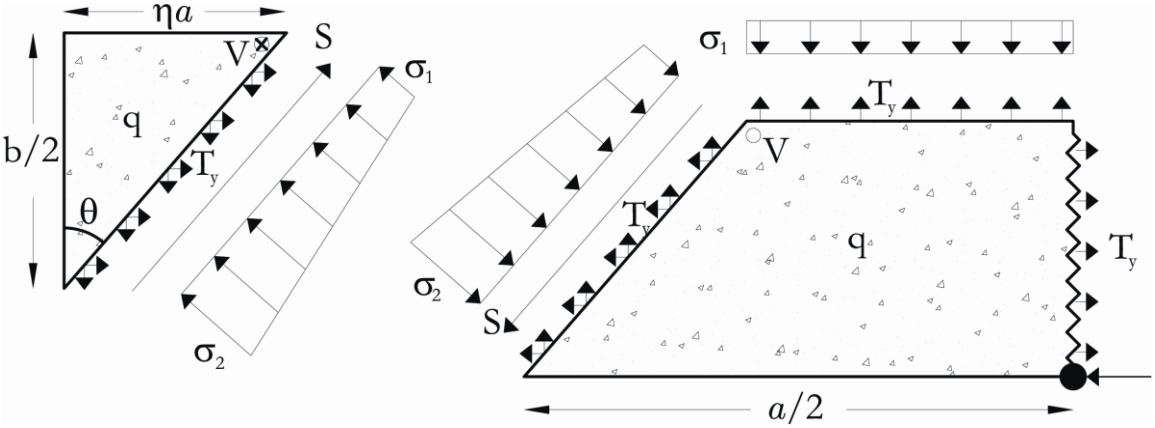

Figure 6: Stress distribution over a quarter slab for distributed concrete compression

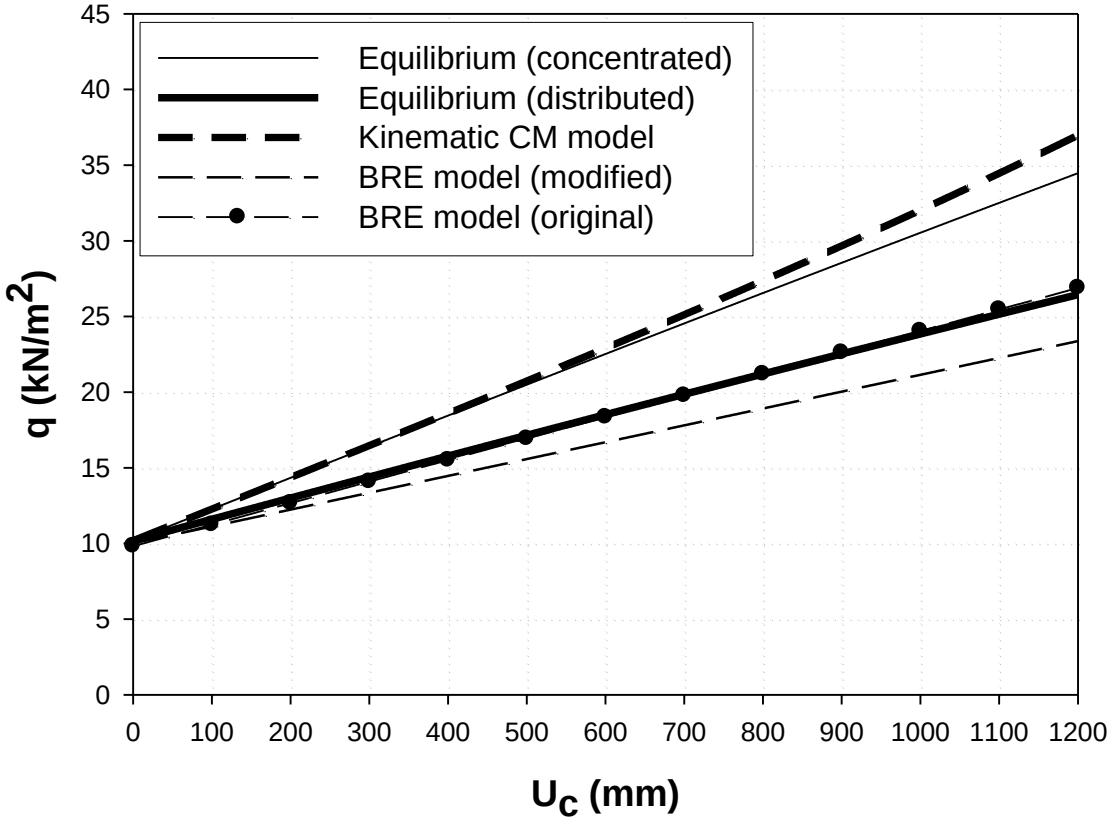

Figure 7: Load deflection response using kinematic and equilibrium approaches

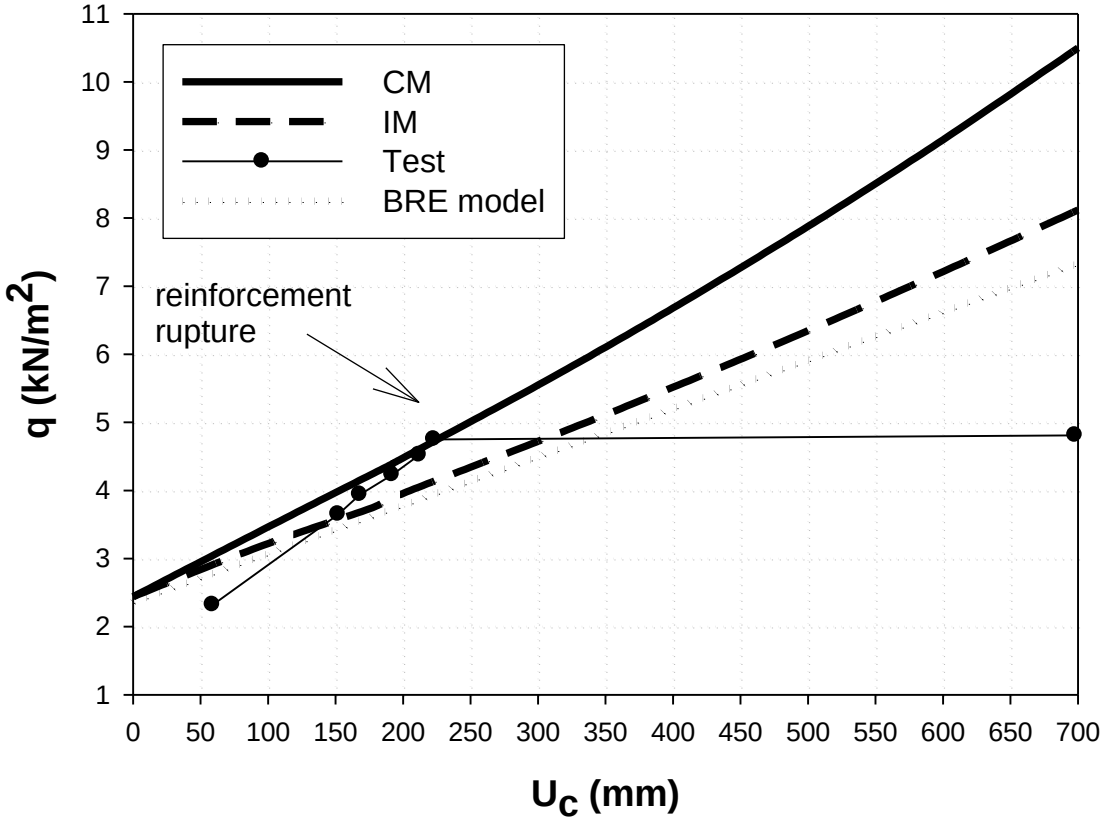

Figure 8: Load deflection response comparison between models and test results

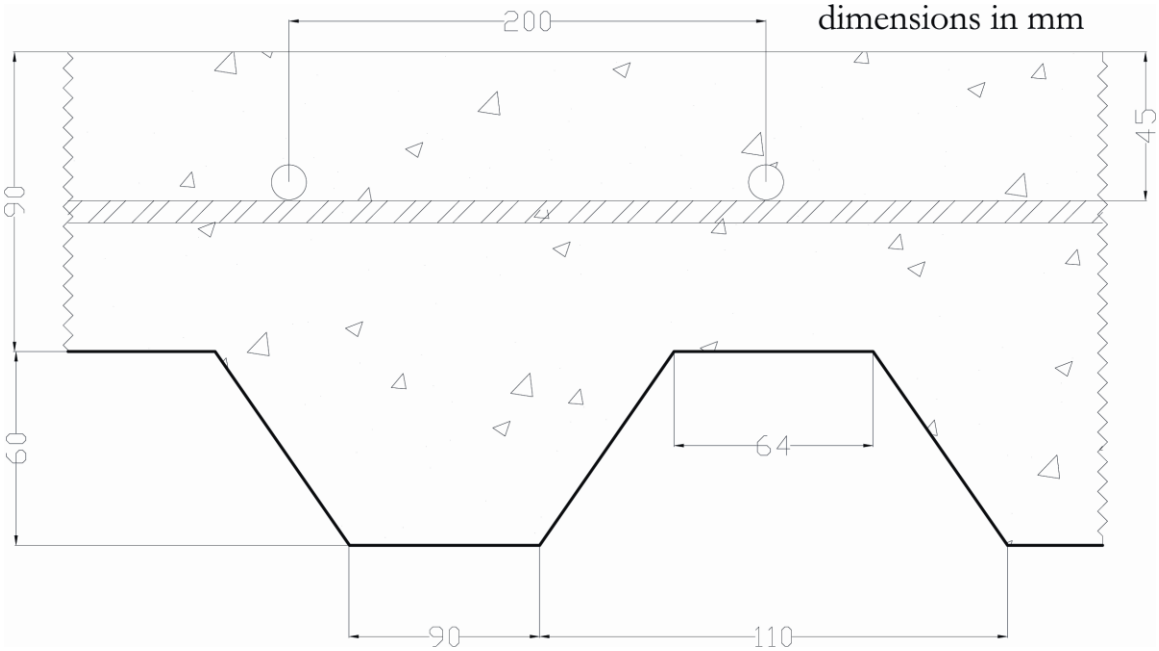

Figure 9: Cross-section through the thickness of a slab typically used in office buildings

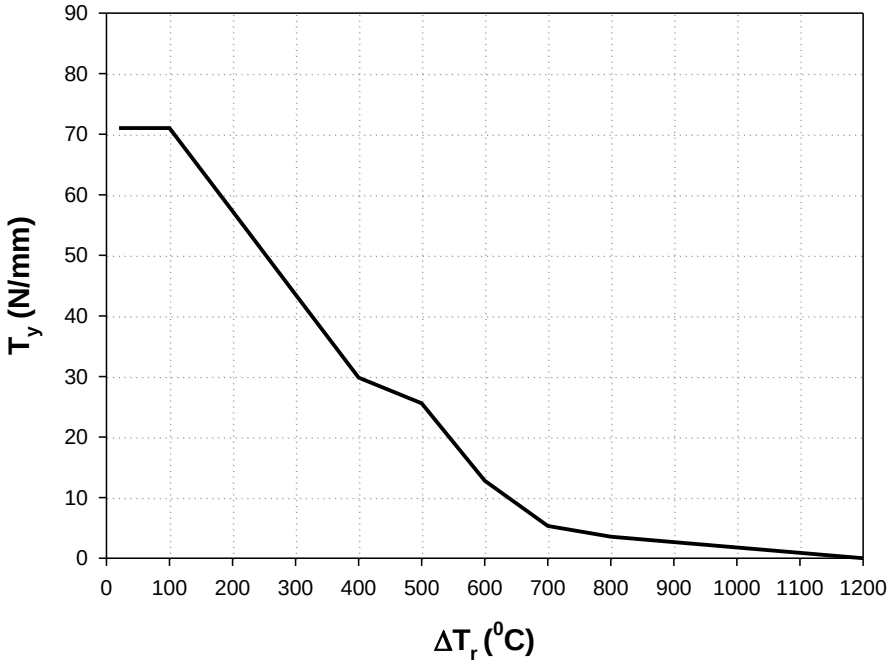

(a) T_y

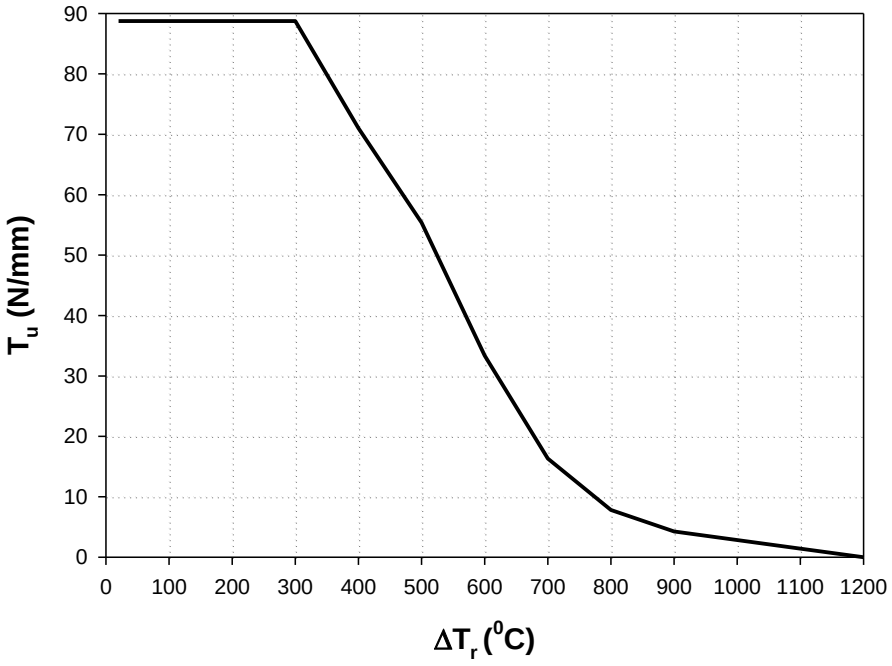

(b) T_u

Figure 10: Variation of yield and ultimate reinforcement force with temperature

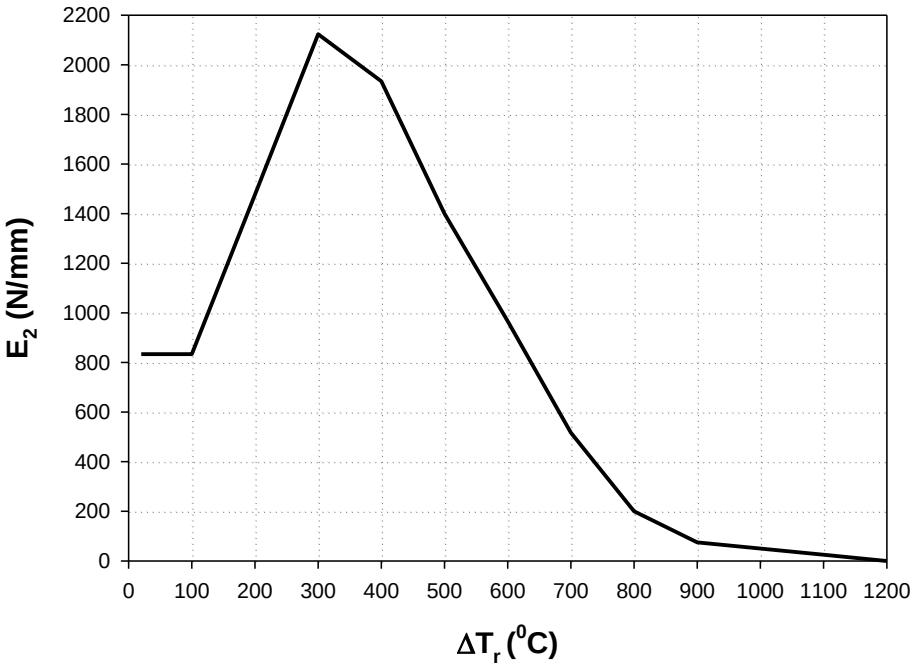

(a) E_2

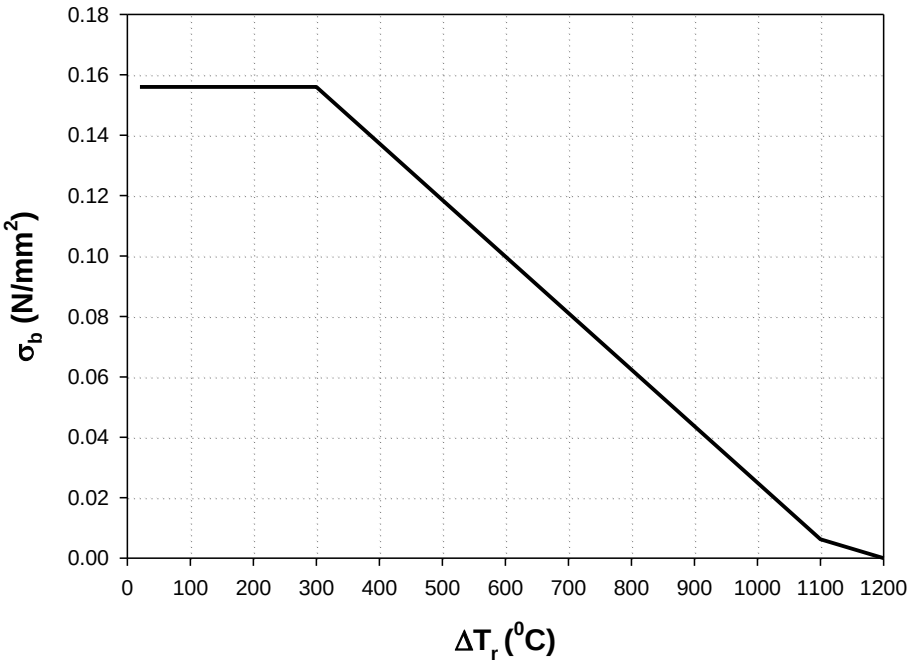

(b) σ_b

Figure 11: Variation of steel hardening modulus and bond strength with temperature

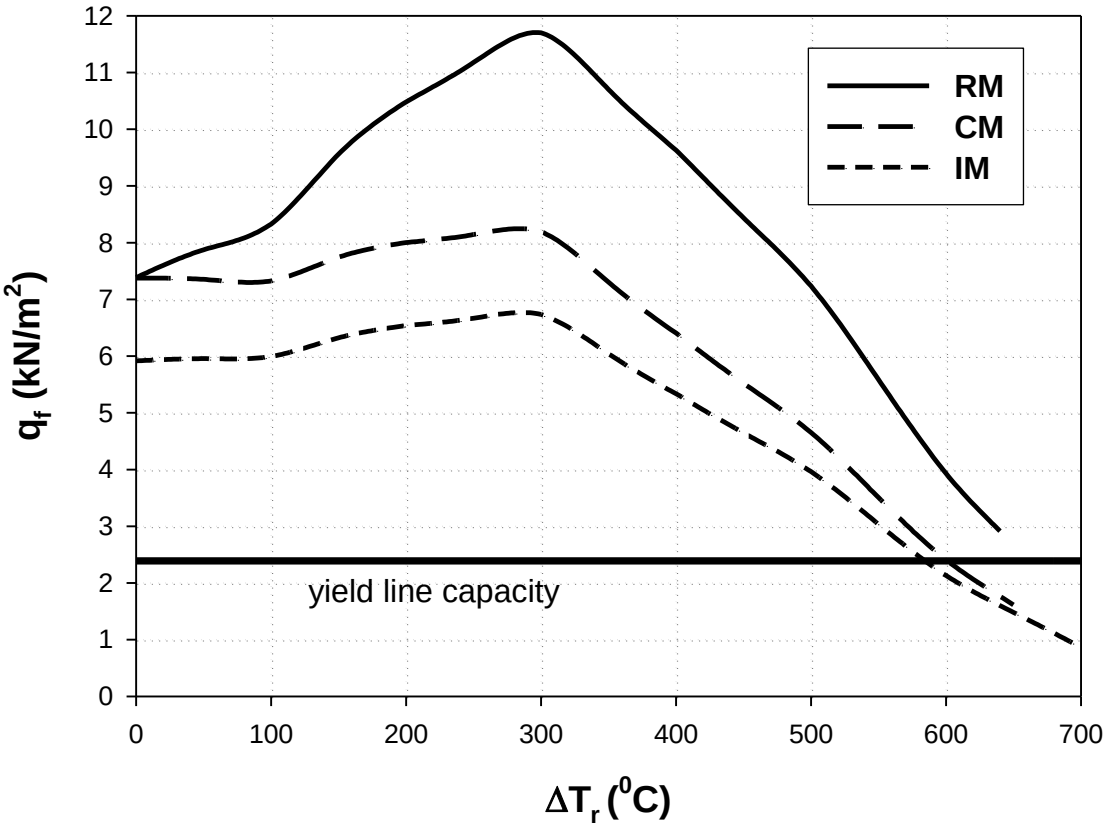

Figure 12: Failure load-temperature variation for b=4.5m

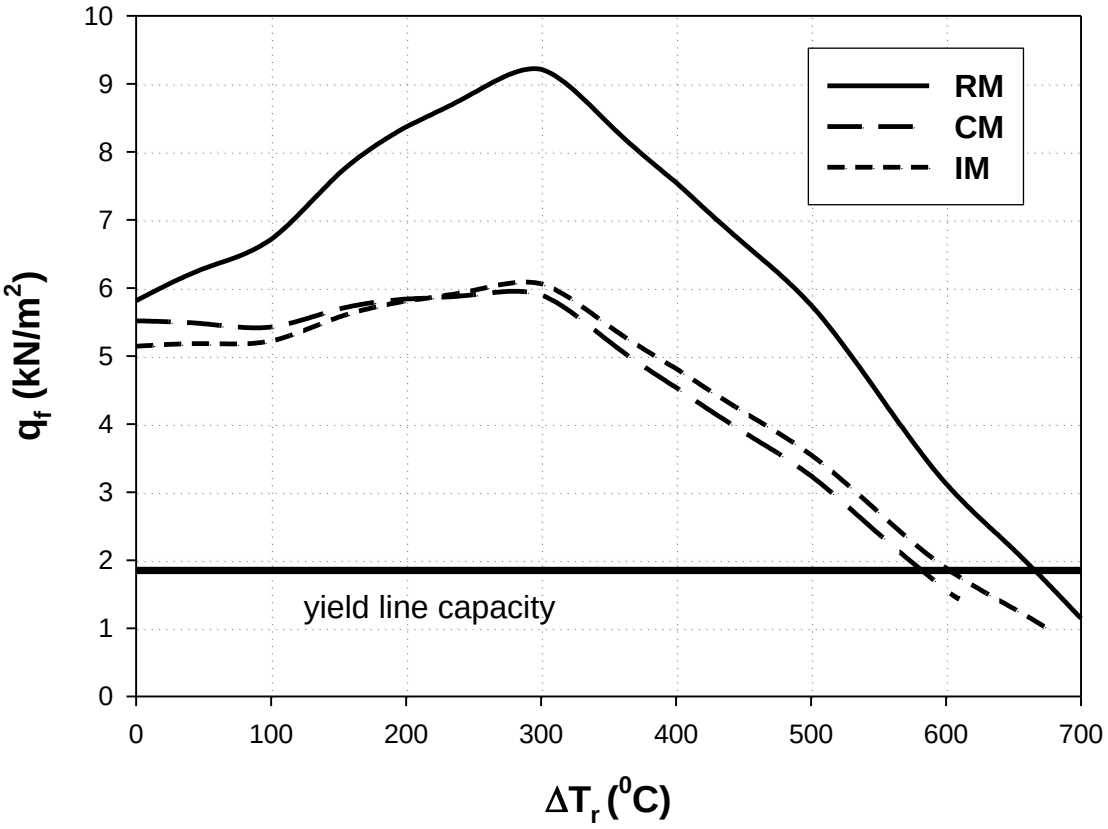

Figure 13: Failure load-temperature variation for b=5.5m

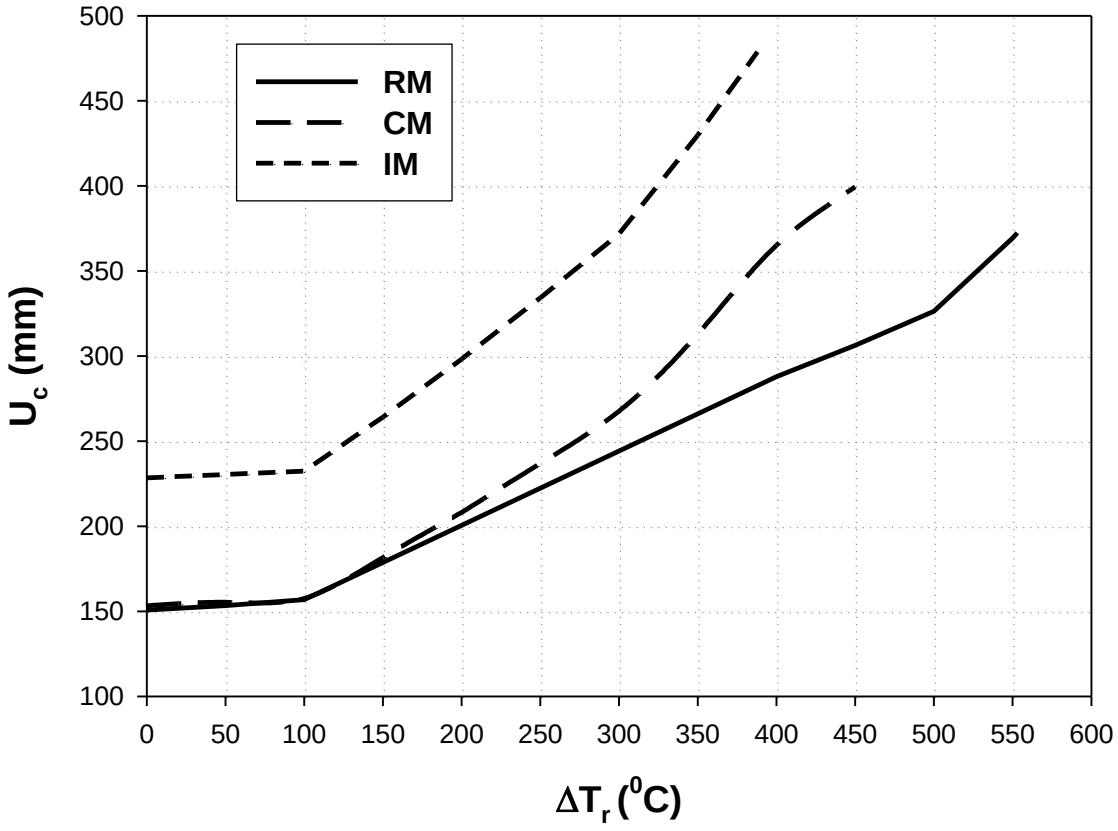

Figure 14: Deflection-temperature response for b=4.5m

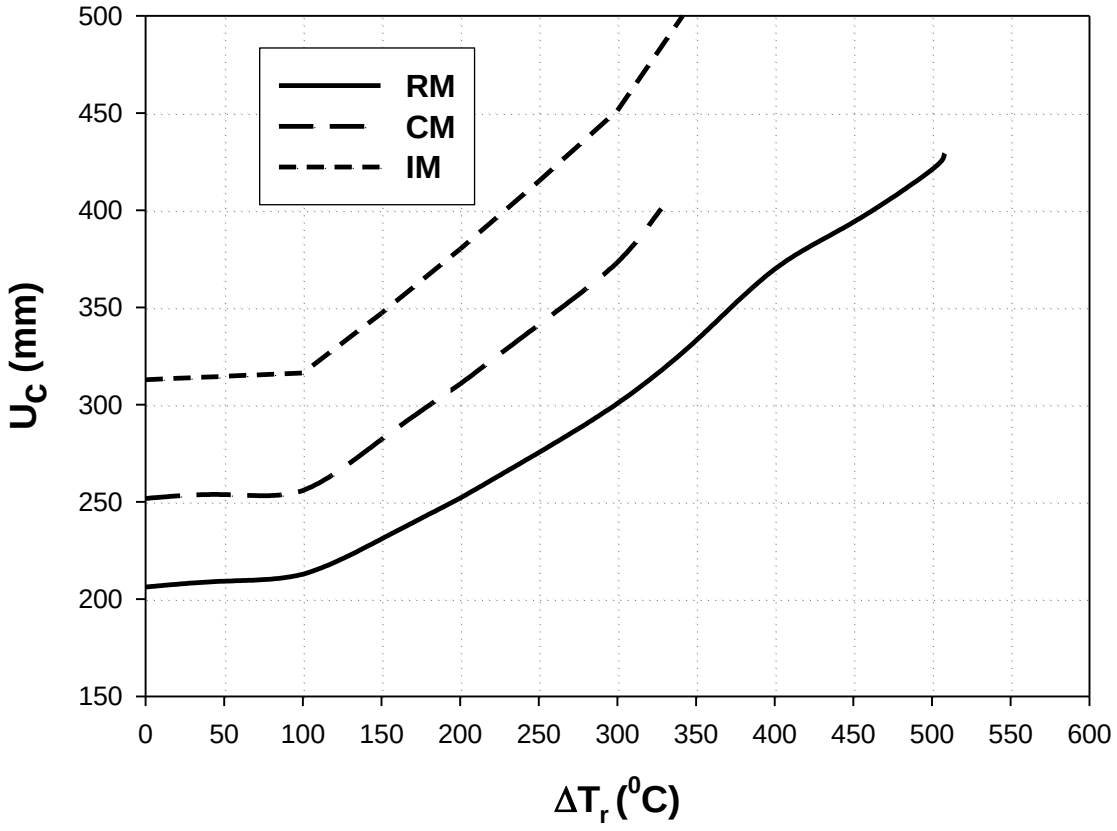

Figure 15: Deflection-temperature response for b=5.5m

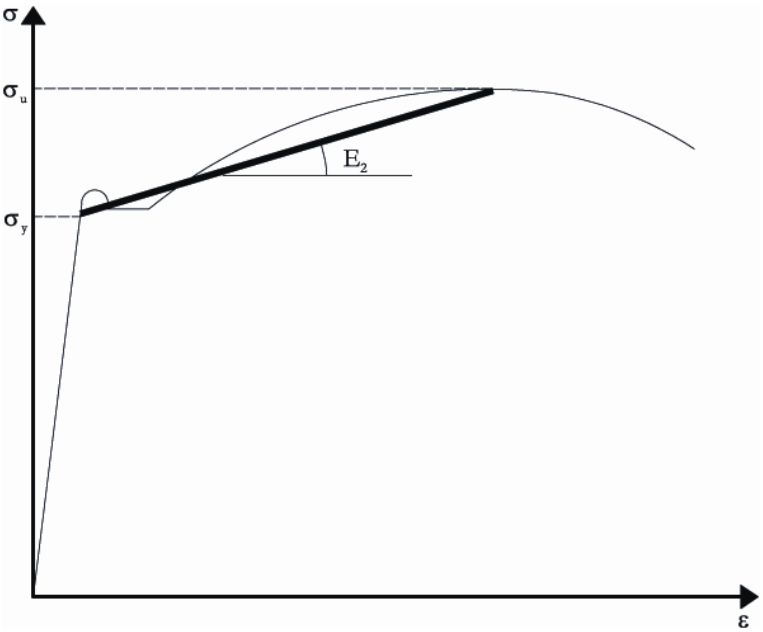

Figure 16: Schematic steel stress strain response

References

[1] Izzuddin, B. A. *Nonlinear dynamic analysis of framed structures*. PhD thesis, Imperial College, London, 1991.

[2] Izzuddin, B. A. and Elghazouli, A. Y. Failure of Lightly Reinforced Concrete Members under Fire. I: Analytical Modelling. *Journal of Structural Engineering, ASCE*, 130(1):3-17, 2004.

[3] Omer, E., Izzuddin, B. A. and Elghazouli, A. Y. Failure of Unrestrained Lightly Reinforced Concrete Slabs Under Fire – Part I: Analytical Models, 2009, (*Companion Paper*).

[4] Izzuddin, B. A., Tao, X. Y. and Elghazouli, A. Y. Realistic modelling of composite and reinforced concrete floor slabs under extreme loading. I: Analytical method. Journal of Structural Engineering, ASCE, 130(12):1972–1984, December 2004.

[5] Izzuddin, B.A. ADAPTIC User Manual, Imperial College, London (http://spiral.imperial.ac.uk/), 2009.

[6] Elghazouli, A. Y. and Izzuddin, B. A. Failure of Lightly Reinforced Concrete Members under Fire. II: Parametric studies and design considerations. *Journal of Structural Engineering, ASCE*, 130(1):18-31, 2004.

[7] Bailey, C. G. Membrane action of unrestrained lightly reinforced concrete slabs at large displacements. *Engineering Structures*, 23:470-483, 2001.

[8] Bailey, C. G. and Moore, D. B. The structural behaviour of steel frames with composite floorslabs subject to fire: Part1: Theory. *The Structural Engineer*, 78(11):19-27, 2000.

[9] Hayes, B. Allowing for membrane action in the plastic analysis of rectangular reinforced

concrete slabs. *Magazine of concrete research*, 20(65):205-212, 1968.

[10] Bailey, C. G., White, D. S. and Moore, D. B. The tensile membrane action of unrestrained composite slabs simulated under fire conditions. *Engineering Structures*, 22(12):1583-1595, 2000.

[11] Omer, E., Izzuddin, B. A. and Elghazouli, A. Y. Failure of Lightly Reinforced Concrete Floor Slabs with Planar Edge Restraints under Fire. *Journal of Structural Engineering, ASCE*, Vol. 135, No. 9, September 2009, pp. 1068-1080.

[12] Eurocode4. *Design of composite steel and concrete structures: Part 1.2:General rules-Structural fire design*. European Committe for Standardization, Brussels, 2005. BS EN 1994-1-2.

[13] *BS 8110 Structural use of concrete: Part 1: Code of practice for design and construction*. BSI, London, 1997.

[14] Eurocode1. *Actions on structures: Part 1.1:General actions-Densities, self weight, imposed loads for buildings*. European Committe for Standardization, Brussels, 2002. BS EN 1991-1-1.

[15] Eurocode1-UK-NAD. *UK National Annex to Eurocode 1:Actions on structures: Part 1.1:General actions-Densities, self weight, imposed loads for buildings*. British Standards Institution, London, 2005. NA to BS EN 1991-1-1.